A study of pulsating flow in automotive catalyst systems

Benjamin, S.F. , Roberts, C.A. and Wollin, J.

Original citation & hyperlink:
Benjamin, S.F. , Roberts, C.A. and Wollin, J. (2002) A study of pulsating flow in automotive catalyst systems. Experiments in Fluids, volume 33 (5): 629-639.
http://dx.doi.org/10.1007/s00348-002-0481-0

FINAL VERSION (REVISED) SENT TO EDITOR 7 FEB 02

A Study of Pulsating Flow in Automotive Catalyst Systems

S. F. Benjamin, C. A. Roberts and J. Wollin

School of Engineering
Coventry University, Coventry CV1 5FB

ABSTRACT

Conversion efficiency, durability and pressure drop of automotive exhaust catalysts are dependent on the flow distribution within the substrate. This study examines the effect of pulsating flow on the flow distribution within these systems. The flow distribution was measured for a range of flow rates at pulsation frequencies of 16, 32, 64 and 100 Hz. It was shown that the flow uniformity at 16 Hz was similar to the steady equivalent whereas improved uniformity was seen at the higher frequencies resulting in a reduced pressure drop. It was further found that flow maldistribution under pulsating conditions was less sensitive to increases in flow rate compared to steady state flow. Downstream of the monolith strong pulses were observed although the pulse shapes changed across the substrate diameter. Flow maldistribution correlated well with a non dimensional parameter derived from the inlet flow velocity, pulsation frequency and diffuser length.

NOMENCLATURE

A	Cross sectional area [m^2]
d	Diameter [m]
f	Frequency [Hz]
L	Diffuser length [m]
$\dot{m}$	Mass flow rate [kg/s]
Re	Reynolds number in inlet pipe
T	Period, 1/f, [s]
U_e	Mean velocity at the rear of substrate [m/s]
U_{in}	Mean velocity in the inlet pipe [m/s]
U_l	Local axial velocity at rear of substrate [m/s]
μ	Dynamic viscosity [kg/m s]
ρ	Air density [kg/m^3]
ψ	Non-uniformity index
σ_V	Variance of velocity [m/s]

Reynolds nr. $\mathrm{Re} = \dfrac{\rho \times U_{in} \times d}{\mu}$

Non-dimensional group $J = \dfrac{U_{in} \times T}{L}$

Correspondence to: Dr S. F. Benjamin
Coventry University, School of Engineering
Coventry, CV1 5FB, U.K.

1 Introduction

Ever more stringent emission regulations within the automotive industry have led to a wide spread use of exhaust catalyst aftertreatment systems. The active catalyst material currently most frequently used is a mixture of Palladium, Platinum and Rhodium dispersed in an aluminium oxide wash coat. This wash coat is used to coat a monolithic ceramic or metallic substrate, comprising of many parallel channels, which provides a high surface area. At ambient temperatures the emissions pass untreated through the catalyst system. It is not until the temperature has reached about 500K that reactions occur. External and internal substrate geometries vary greatly. External geometries depend on engine size, designated geographical market and vehicle packaging. The channel geometry depends on the type of substrate. The most common channel shape for ceramic substrates is currently square channels with a 1 mm hydraulic diameter although triangular and hexagonal shapes are available. For metallic substrates the predominant cross sectional shape is sinusoidal due to the winding technique used when manufactured. Current production substrates feature a cell density of between 31-93 cells/cm^2 although prototype substrates with cell densities up to 248 cells/cm^2 are being developed.

Pressure drop considerations dictate the use of short substrates. This means that their diameter in most cases is significantly larger that the up-stream exhaust pipe. Packaging constraints often compromise the geometry of the expansion. Increasingly reduced space envelopes require short abrupt expansion with total diffuser angles of 60-80 degrees. These wide-angle diffusers cause a flow separation in the diffuser throat, which produces a maldistributed flow impinging on the front face of the substrate as found by Kim et al. (1995) and Wendland and Matthes (1986). Maldistributed flow adversely affects conversion efficiency (Howitt and Sekella (1974), Comfort (1974)), catalyst durability (Will and Bennett (1992)) and pressure loss (Benjamin et al. (1996)). Concentrated heat flux caused by maldistributed flow could however potentially contribute to reducing the light-off time as indicated by Martin et al. (1998). Knowledge of the flow distribution is clearly of importance when designing catalyst systems.

Flow distribution studies have mostly been performed under conditions of steady flow. This may be a reasonable approximation for some under body systems but is certainly invalid for close coupled catalysts (CCC) positioned close to the engine. One dimensional pulsating flow studies in engine systems have been the subject of extensive research over several decades. The book by Blair (1999) provides a comprehensive review of this subject. The contents describe how wave dynamics affects the mass flow through the engine and concerns wave propagation, transmission and reflection in inlet, exhaust pipes and

system components. Flow details in complex components are not considered, the primary interest being their effect on wave dynamics. An example of this can be found in the work of Carberry et al (1995) who measured transmission and reflection coefficients of catalyst elements in a one dimensional single shot rig. Such information can be utilised in a one dimensional engine system model. There has been comparatively little work published on the three dimensional unsteady flow field within CCC or underbody catalyst systems. CCC systems typically feature each exhaust port discharging directly into the upstream diffuser. With underbody systems the exhaust ports usually discharge into a common downpipe prior to entering the diffuser.

Park et al (1998) measured the flow field in a dual monolith CCC fitted to a firing engine using laser doppler velocimetry (LDV). The four exhaust ports discharged at different locations within the upstream diffuser. Velocity measurements were made in one of the exhaust ports, at various locations within the upstream diffuser and between the oval shaped monoliths. At 2000 rpm and half load primary exhaust pulses of magnitude 120-130 m/s were observed in the port corresponding to the initial exhaust blow down. Subsequent secondary pulses were also observed. Measurements within the diffuser showed a complex time varying velocity field with. mean velocities within the range -20 to 20 m/s whereas within the gap between the monoliths they ranged from –3 to 10 m/s. Their major conclusion was that the primary pulse from each cylinder largely governs the flow characteristics within the catalyst.

Hwang et al (1995) studied the internal flow characteristics of an oval dual monolith CCC using LDV and high speed flow visualisation. Ensemble averaged LDV measurements were taken 2.5 cm in front of the first monolith and in the midsection between the monoliths under unsteady flow conditions. A production intake and exhaust manifold and exhaust system was used. Pulses were generated by blowing air through a cylinder head with the exhaust flow simulated by operating the exhaust valves with a cam driven by a DC motor. The main conclusion from this study was that dynamic flow characteristics were different from those under steady flow conditions. Each cylinder exhausted into different regions of the converter. The midsection between the monoliths had a more uniform flow pattern but pulses were still evident at high flow rates.

Bressler et al (1996) generated pulses using a rotating chopper disk which was connected in turn to each of four exhaust ports to a circular CCC which appears to discharge directly to atmosphere. A tracer gas was used to identify the contribution to the flow across the rear of the monolith from each of the ports. Idealised "trapezoidal" pulse profiles were generated. They found that the flow distribution across the

monolith varied with load but was independent of engine speed at a given load. They concluded that the important factor governing flow uniformity was the ratio of the swept cylinder volume to the volume in the upstream diffuser. When this was low port flow interference (mixing) occurred in the upstream diffuser thus providing a more uniform flow distribution across the monolith. Under such conditions the flow was more uniform than under steady flow.

Zhao et al. (1995) undertook experimental studies of pulsating flow on dual monolith underbody systems on a firing engine fitted with a production exhaust. LDV was used to measure the mean velocity across the major and minor axes of an oval converter 1 mm from the front face of the monolith. Observations of the velocity probability density function (PDF) at the centre location showed that at low rpm a bi-modal distribution was evident suggesting to the authors that the flow was pulsating. At higher engine speed (frequency) the PDF was flatter suggesting a quasi-steady flow. They also concluded that the spatial velocity distribution under firing conditions was more uniform than for steady flow. In a later study Zhao et al. (1997) obtained cycle resolved LDV measurements on a firing engine to study pulse shapes within a catalyst system. For this study a different engine was used and it is not clear if either a single or twin monolith oval design was installed. Pulse shapes were measured on the axis upstream and 5 mm downstream of the monolith. Periodic pulse shapes typical of those generated by an engine were observed up-stream of the substrate whereas downstream they were absent. The explanation offered was that the monolith was acting as a muffler to filter out the pulsations in the exhaust flow.

Most of the studies reported in the literature were performed on "production type" systems where a limited number of parameters were investigated. A common feature is that pulsating flow will provide a different flow field to that observed under conditions of steady flow. This study is aimed at providing a more fundamental investigation by focusing on simple yet representative systems and systematically varying control parameters. To achieve this the experimental work has been undertaken on an iso-thermal flow rig using a mechanical pulse generator coupled to 2D axially symmetric catalyst systems. This was done so as to avoid the complications and uncertainties often associated with experimental work using firing engines. Axially symmetric systems were used because they are expected to contain many of the important flow features found in more complex systems and at the same time require fewer measurements to characterise the flow. In addition the computational resources to simulate 2D regimes are far less demanding. To characterize the flow a parameter $J=U_{in}/Lf$ (reciprocal of the Strouhal number) can be defined which represents the ratio of the pulse period to the residence time in the diffuser. In this study J varies from 1-30. Real pulse trains vary widely depending on engine type and operating condition. For the

purposes of this study it was decided to study pulses of approximately sinusoidal shape with an amplitude/mean ratio of approximately one. This is believed to be a reasonable if idealised representation and forms a good basis for future studies of more complex systems. The work described in this paper is part of a program aiming to provide experimental data for verification of a computational fluid dynamics (CFD) computer model. Pulsating flow is clearly of interest in exhaust systems and a complete model of an autocatalyst system must predict the spatial and temporal flow distribution correctly across the catalyst in order to provide accurate predictions for temperature and conversion efficiency. Such flow measurements are reported in this study.

2 Experimental method

2.1 Description of the test rig

A schematic layout of the iso-thermal test rig used in this study can be seen in figure 1 with details of the pulse generator and catalyst assembly shown in figure 2. The test rig is supplied with compressed air from two receivers via a main valve (1). A pressure gauge (2) monitors the supply pressure, which is reduced from ~6.9x10^5 Pa to ~2.8 x10^5 Pa by a valve (3). A second pressure gauge monitors the up-stream rig pressure (4). A filter (5) is used to avoid oil contamination. The mass flow rate is controlled by an adjustment valve (6). A safety relief valve rated at 5.5 x10^5 Pa is used to avoid damage to the rig (7). Rig pressure (less than 10^5 Pa) is monitored by a pressure gauge (8). For steady flow conditions, flow rate is measured using a calibrated viscous flow meter (VFM) (10). Up-stream of the VFM is a 50 mm flow straightener (9) used to ensure a smooth inlet to the VFM. The viscous flow meter is connected to a digital manometer FCO16 from Furness Controls. A plenum incorporating a flow straightner (11) is used to avoid swirl components in the flow and a contracting nozzle (12) produces a uniform velocity profile at the diffuser inlet under steady flow conditions. The pulsations are achieved using a pulse generator (13) of which an exploded schematic can be seen in figure 2. A tube (14) was used to hold flow straighteners to achieve uniform flow as described below. 60-degree (15) and 180 degree total angle axially symmetric diffusers were used in the experiments. The length of the 60 degree diffuser was 61.5 mm. Three 180 degree diffusers were tested of varying length, 61.5, 79.85 and 119.15 mm. The inlet pipe diameter, on which all Reynolds numbers are based was 48 mm. All the diffusers feature a 20 mm inlet section prior to the diffuser throat. On the test substrate (16) an outlet sleeve (17) was used to avoid entrainment of

surrounding air. Two ceramic substrates were used in this study of lengths 152 mm and 102 mm. Both substrates had a nominal cell density of 62 cells/cm^2, square channels and a diameter of 118 mm.

The pulse generator consists of a 12 mm aluminium housing case in which a cast iron rotor plate is revolving. The plate interrupts the flow periodically. The plate can house four inserts with shaped holes to enable easy modification of the generated pulse shape. The configuration used in these experiments was one hole per insert so that the rotor plate had 45 degrees of closed surface followed by 45 degrees open. The inlet tube diameter that coincides with the plate edge when the duct hole is half open is defined as the x-axis (horizontal). The diameter at right angles to this is defined as the y-axis (vertical).

For steady flow the nozzle provided a uniform flat velocity. However during commissioning of the pulse generator it was found that the flow after the nozzle was not uniform (Wollin (2001)). A high velocity surge was observed as the flow path through the pulse generator was opened. This surge was significant at the upper end of the flow rate range of interest, but was less apparent at lower mass flow rates. Flow straighteners were added to the test rig to achieve flow uniformity at inlet to the catalyst configuration. The straighteners were made from 62 cells/cm^2 ceramic substrate and were placed downstream of the rotating pulse generator. Experiments with the 152 mm substrate showed that the flow straightener configuration seen in figure 3A produced axially symmetrical uniform velocity profiles for 64 and 100 Hz at all Reynolds numbers. For the experiments at 16 and 32 Hz a third 50 mm flow straightener was added as seen in figure 3B. For the 102 mm substrate all experiments were carried out with the triple flow straightener.

Inlet velocity profiles measured using the three substrate straightener at a Re of ~80000 and a frequency of 32 Hz can be seen in figure 4. The measurements were taken 30 mm downstream of the last substrate, i.e. 260 mm from the exit plane of the pulse generator. It can be seen that without the flow straighteners the flow distribution was clearly not axially symmetric. The flow distribution with the flow straighteners added was found not to be ideal but with significantly improved flow symmetry. The flow symmetry was believed to be very important since a different extent of flow separation would otherwise be created. It was found that for lower flow rates and higher frequencies the flow distribution at the inlet improved both with and without the flow straighteners. As a check on the flow symmetry, profiles at the rear of the substrate were taken along several diameters.

2.2 Experimental measurements

The flow distribution was determined by measuring velocity profiles at inlet to the diffuser and at the rear of the substrate. For the velocity measurements a TSI IFA300 Constant Temperature Hot Wire Anemometry (HWA) system was used. The system comprises a main unit with the HWA bridges, a 2D traverse and the Thermal Pro software to control and acquire data. The probes were 1.25 mm length 5 μm Tungsten/Platinum wire probes, calibrated using a fully automatic TSI 1129 calibrator. The velocity profiles measured downstream of the substrate were measured within a sleeve 30 mm from the outlet face. Haimad (1997) had shown that this distance was necessary in order to avoid jets from individual channels. The measurements were taken without an exit cone since Lemme and Givens (1974) showed this to have a very small effect on the steady state flow distribution. Steady flow experiments were also performed using a 0.5 mm total head pitot tube. Good correlation was seen which confirmed the calibration of the HWA probe. As well as logging profiles of mean velocity values, the TSI HWA system was able to provide traces of the pulse shapes and statistical information such as standard deviation. The 2D automatic traverse system enabled rapid velocity profiling to be carried out at increments of 2.5mm. Some measurements of inlet velocity, however, where the flow profile upstream was investigated with the catalyst configuration in place, necessitated manual positioning of the anemometer probe. A sampling size of 2048 points was used for all velocity measurements downstream of the catalyst. For the steady state experiments and those at 16 and 32 Hz the sampling rate was 1000 Hz whereas at 64 and 100 Hz it was set to 2000 and 4000 Hz respectively.

3 Experimental Results

Measurements were taken for Re numbers ranging from 20000 to 110000. The pulsation frequency was 16, 32, 64 and 100 with a ± 3 Hz tolerance in all experiments. The inlet velocity profiles were measured 45 mm up-stream of the diffuser throat. It was found the presence of the diffuser and substrate did not affect the flow distribution, i.e. the velocity profile shape supplied by the test rig. The Re number at which the experiments were performed was calculated through integration of the velocity profiles at the rear of the substrate. Variations in Re number compared to the nominal value were found initially. This was found to be caused by the FCO16 manometer, which was used to measure the pressure drop across the VFM, giving incorrect readings under pulsating condition due to its low sampling rate. To circumvent this the flow rate was set by monitoring the velocity with a HWA probe situated 45 mm upstream of the diffuser throat.

3.1 Flow Distribution

To evaluate the effect of pulsation frequency and mass flow rate a non-uniformity index was devised. In practice it is the variance of the flux of any variable through the monolith (species concentration, enthalpy, etc) which is important and so in keeping with this the non-uniformity index was calculated using the mass flow weighted velocity integrated over the substrate face. The variance of the velocity, σ_V, is defined according to equation 1. This results in a non-uniformity index ψ, over the cross section of the substrate according to equation 2. A non-uniformity index of zero means that the flow distribution is uniform across the substrate.

$$\sigma_V = \frac{1}{\dot{m}} \int_A |U_i - U_e| \delta \dot{m} \qquad 1$$

$$\psi = \frac{\sigma_V}{U_e} \times 100 \qquad 2$$

Figure 5A shows the variation in ψ with Re and frequency for the 152 mm substrate using the 60 degree diffuser. Maldistribution is seen to increase with Re. This is an established phenomenon for steady flow (for example, see Benjamin et al (1996)) and is a consequence of the high inertia inlet flow separating at the diffuser throat. Figure 5A shows this also occurs with pulsating flow although ψ is clearly less sensitive to Re when compared to steady state conditions. Figure 5B shows ψ against Re number for the 102 mm and 152mm substrates. The effect of a shorter substrate is that it reduces the downstream resistance, producing a more maldistributed flow. Figure 5C shows ψ against Re number for the 180 degree and 60 degree diffuser both using the 152mm substrate. A 180 degree diffuser causes total flow separation in the diffuser throat and is therefore expected to result in an increased non-uniformity when compared to the 60 degree diffuser. This is verified in figure 5C.

As the largest difference in ψ occurs at the highest flow rate velocity profiles at different frequencies are only shown at high Re. Figure 6 compares the velocity profiles at different frequencies with that at steady state. It can be seen in figure 6A that good flow symmetry was achieved for both the steady and pulsating case. Therefore for clarity only the velocities along the x-axis have been plotted in the remaining figures. The flow distribution at 16 Hz is similar to the steady state cases. As the frequency increases, however an

improved flow distribution is observed. These beneficial effects were believed by Zhao et al. (1995) to be caused by pulsations acting similarly to large-scale turbulence, enhancing mixing.

3.2 Pulse shapes

Examples of typical pulse shapes observed in the centre of the inlet pipe are shown in Figures 7 and 9. The pulse shapes at the inlet for a Re of ~40000 and frequencies of 16, 32, 64 and 100 Hz can be seen in figure 7. The pulse shapes at the inlet for 32 Hz and Re of ~20000, ~40000, ~60000 and ~80000 can be seen in figure 9. The amplitude is seen to be of the same order as the mean and the pulse is of approximately sinusoidal shape. There was some evidence of pulse shape change across the diameter, observed as a slight "leaning" of the pulse. This was dependent upon proximity to the areas where the duct first opens and finally closes. In figure 7 it can be seen that the pulse shapes are very similar. The only exceptions were for 16 Hz at low Re numbers which featured a double peak and for the higher frequencies at all Re numbers where secondary minor peaks could be seen when the pulse generator was closed. The double peak for the 16 Hz case is believed to be due to a surge when the flow path opens which is stronger than the main flow rate. This is further confirmed since it disappears as the frequency and flow rate is increased. The minor secondary peak seen for the 64 and 100 Hz cases are most likely caused by leakage as a consequence of pressure build up upstream of the pulse generator during the closed period.

The pulse shapes at the exit were found to change across the diameter of the substrate with Re and frequency. Figures 8 and 10 show the exit pulse shapes 20 mm from the wall and at the axis. Figure 8 shows pulses at Re ~ 40000 and frequencies of 16, 32, 64 and 100 Hz. Figure 10 shows pulses at 32 Hz for a range of Re. It can be seen that the mean velocity of the pulse at the axis is elevated compared with the pulse at the wall as Re increases at a fixed frequency or as frequency decreases for a given flow rate. This is consistent with the flow distribution trends observed in figure 5.

The observation by Zhao et al. (1997) that the pulses are eliminated has however not been verified. In that study engine pulses of less clearly defined shape were generated and observations were only reported along the central axis. In this study, strong pulses of approximately sinusoidal shape were input to the system. Under firing conditions with high temperatures substrate resistance increases and this also may account for the differences between observations in the two studies.

3.3 Pressure drop measurements

Pressure drop measurements were taken for both steady and pulsating flows using the 60 degree diffuser and 152 mm substrate. The pressure for steady state conditions was measured using a Digitron P200 (0-$2x10^4$ Pa) micro manometer connected to a static pressure tapping 45 mm up-stream of the diffuser throat. For pulsating flow, two piezo ceramic pressure sensors from Druck were used, their frequency being limited by the amplifier response (2kHz). The PMP4010 sensors had a pressure range of –7000 to 7000 Pa gauge. The sensors had an integrated amplifier which means that a –5 to 5 volt output signal was obtained. The signal from the transducers was taken directly into the A/D board of the IFA300 system. The PMP4010 transducers were powered with 24 volt 700 mAh battery packs. One transducer (P1) was connected 45 mm up-stream of the diffuser throat, in the same plane as the static pressure tapping and hot wire anemometer. The second transducer (P2) was connected 30 mm downstream of the substrate exit face. The mean static pressure drop was obtained by deducting the downstream transducer signal from the up-stream transducer signal and taking the mean of the resulting signal. The velocity trace at the inlet was found to be significantly different from the pressure pulse shape as seen in figure 11A, the difference being attributed to inertia lag, as there is a closer correlation with acceleration. It was also found that the amplitude of the pressure fluctuations increased with pulsation frequency. All the mean static pressure drops plotted against Re can be seen in figure 11B. It can be seen that the pressure drop for different frequencies and flow rates showed the same tendency as the non-uniformity index plotted in figure 5. This suggests that higher pressure losses are closely linked to increased monolith losses associated with maldistributed flow. A similar relationship was established for steady flow by Benjamin et al (1996)

3.4 Ensemble averaged velocity profiles

For further insight into the pulsating flow behaviour in the diffuser it was concluded that instantaneous velocity profiles would be useful. To capture true instantaneous velocity profiles there would be a need for approximately 50 probes in fixed locations at the exit of the substrate, which was not feasible due to

equipment available. Instead the velocity traces collected at each individual traverse location were used. A pulse generator signal was logged simultaneously with the velocity trace and used as a timing signal. It registered zero volts when the flow path through the pulse generator was fully closed and approximately four volts at all other conditions. Using the timing signal the velocity trace at each spatial location was ensemble averaged (minimum of 50 cycles) to minimise any cycle to cycle variations. The ensemble averaged velocity on the axis in the inlet tube 45 mm upstream of the diffuser throat was also recorded. This was used to correlate with the flow distribution measured at the exit to the substrate. Both cases presented are taken over the x-axis at 32 Hz and Re=95800 and 100 Hz and Re=102300.

For the 32 Hz case figure 12A shows the inlet velocity pulse shape and the times corresponding to the velocity profiles shown in figure 12B. The flow distribution becomes very uniform at times corresponding to the maximum inlet velocity, probably because the flow initially remains relatively attached and also redistributes on the front face due to substrate resistance. As more flow enters the diffuser the flow increasingly separates and flows through the central region.

For the 100 Hz case figure 13A shows the inlet velocity pulse shape and the times corresponding to the velocity profiles shown in figure 13B. It can be seen that the flow distribution is more uniform at all times and never reaches the high velocities seen in the 32 Hz case. For a short period of time, around t=0.0095 seconds, the velocities in the outer region are higher than in the centre. This is believed to be due to leakage through the pulse generator when the flow path is closed resulting in intermittent wall jets at higher frequencies.

The reasons for the increase in flow uniformity at higher frequencies are possibly two fold. Firstly, it would seem that at high frequency the flow does not have sufficient time to establish the inertia dominated steady flow regimes associated with high Reynolds number flows, that is separation at the throat and large recirculation zones within the diffuser volume. At low frequency separation at the diffuser inlet may be more likely at the peak of the pulse as the flow is quasi-steady and hence the flow maldistribution may be expected to be similar to that under steady flow conditions as shown in figure 6. Secondly, the enhanced mixing within the diffuser at higher frequencies could also produce flatter profiles. At low values of J there is the possibility of more than one pulse residing in the diffuser volume at any one time leading to pulse interaction and increased mixing. Increasing the residence time in the diffuser (say by increasing the diffuser length) would increase the probability of such an occurrence. There is also a possibility that wave dynamics could be contributing to the increased mixing at higher

frequencies. However pressure measurements recorded 30mm downstream of the rear face of the catalyst (P2 in figure 11A) do not indicate any strong reflections from the open end of the sleeve and it is therefore concluded that such effects are probably secondary.

3.5 Non-dimensional correlations

The observation of improved flow profiles as Re reduces and frequency increases suggests that there is a functional relationship between the maldistribution index and these variables. Clearly the length of the diffuser is also important as mentioned above. To examine if general relationships could be derived two additional 180 degree diffusers were tested. The standard diffuser length (L0) is 61.5 mm long and the additional diffusers were of lengths 79.85 (L1) and 119.15 mm (L2). Velocity profiles for L1 and L2 were taken for high Re in the range of ~70000-110000 for all the frequencies. The results have been plotted in figure 14A as non-uniformity index against the non-dimensional parameter, J. The results collapse reasonably well when plotted in this form. Figure 14B shows the data for the 60 degree diffuser and 152 mm substrate plotted similarly. Such correlations could form a useful basis for design engineers faced with the task of reducing flow maldistribution in autocatalyst systems.

4 Conclusion

This study has examined the effect of pulsating flow within automotive catalyst systems. The flow distribution as exhibited by velocity profiles at the substrate exit has been studied. The effect on pulse shape of passage through the system has also been examined.

With pulsating flow the flow maldistribution is less sensitive to Re when compared with steady state conditions. For the same flow rate the flow distribution at 16 Hz was similar to that with steady flow whereas at the higher frequencies much greater flow uniformity was observed. As a consequence of this pressure drop reduced as frequency increased. Flow uniformity also increased with substrate resistance.

Downstream of the monolith strong pulses were observed but the pulse shapes changed across the substrate diameter. On the axis the mean velocity was found to be generally elevated above that at the wall at low frequency and high flow rate.

Profiles deduced from ensemble averaged velocities showed that at high frequency the velocity profiles were relatively flat throughout a pulse cycle in contrast to those observed at a lower frequency. It would seem that at high frequency the flow does not have sufficient time to establish the inertia dominated steady flow regimes associated with high Re flows, that is separation at the throat and large recirculation zones within the diffuser volume. Enhanced mixing at higher frequencies within the diffuser could also produce flatter profiles.

Maldistribution correlated well with a non dimensional parameter J derived from the inlet flow velocity, pulsation frequency and diffuser length. Such correlations could form a useful basis for design engineers faced with the task of reducing flow maldistribution in autocatalyst systems.

Acknowledgements

We acknowledge ArvinMeritor Limited, Ford Motor Company, Jaguar Cars Limited and Johnson Matthey plc who are supporting this work. We also acknowledge support under the EPSRC-DTI ACCP LINK scheme. We would also like to thank Dr Bryan Philips and Dr Edward Day at Coventry University for technical assistance and Mr David Lloyd-Thomas at Ford Motor Company for valuable discussions.

References

Benjamin S F; Clarkson R J; Haimad N; Girgis N S (1996) An experimental and predictive study of the flow field in axisymmetric automotive exhaust catalyst systems. SAE Int. Spring Fuels and Lubricants Meeting Congress and Exposition. Detroit. USA. SAE paper 961208.

Blair G. P. (1999) Design and Simulation of Four Stroke Engines published by SAE International

Bressler H; Rammoser D; Neumaier H; Terres (1996) Experimental and Predictive Investigation of a Closed Coupled Catalytic Converter with Pulsating Flow. SAE paper 960564. SP-1173.

Carberry B. P., Long P. T., Douglas R. and Fleck R. (1995) The effects of a heated catalyst on the unsteady gas dynamic process. SAE 952141 SP-1112 Design and Emissions of Small Two-and Four-Stroke Engines pp 109-118

Comfort E H (1974) Monolithic Catalytic Converter Performance as a Function of Flow Distribution. ASME Winter Annual Meeting. Paper No.74-WA/HT-30.

Haimad N (1997) PhD Thesis (Coventry University) A Theoretical and Experimental Investigation of the Flow Performance of Automotive Catalytic Converters.

Howitt J S; Sekella T C (1974) Flow Effects in Monolithic Honeycomb Automotive Catalytic Converters. SAE paper 740244.

Hwang K; Lee K; Mueller J; Stuecken T; Schock H J; Lee J-C (1995) Dynamic Flow Study in a Catalytic Converter using Laser Doppler Velocimetry and High Speed Flow Visualisation. SAE paper 950786. SP-1094. 169-186.

Lemme C D; Givens W R (1974) Flow Through Catalytic Converters - An Analytical and Experimental Treatment. SAE paper 740243.

Kim J Y; Kai M-C; Li P; Chui G K (1995) Flow Distribution and Pressure Drop in Diffuser-Monolith Flows. ASME-Journal of fluids engineering. 117. 362-368.

Martin A P; Will N S; Bordet A; Cornet P; Gondoin C; Mouton X (1998) Effect of flow Distribution on Emissions Performance of Catalytic Converters. SAE 980936.

Park S-B; Kim H-S; Cho K-M; Kim W-T (1998) An Experimental and Computational Study of Flow Characteristics in Exhaust Manifold and CCC (closed coupled catalyst). SAE paper 980128.

Wendland D W; Matthes W R (1986) Visualization of Automotive Catalytic Converter Internal Flows. SAE Paper 861554.

Will N S; Bennett C J (1992) Flow Maldistributions in Automotive Converter Canisters and their Effect on Emission Control. 1992 SAE paper 922339. 183-210.

Wollin J. (2001) A Study of Pulsating Flow in Automotive Exhaust Catalyst Systems. PhD thesis (submitted). Coventry University.

Zhao F-Q; Li L; Xie X; Lai M-C (1995) An Experimental Study of the Flow Structure Inside the Catalytic Converter of a Gasoline Engine. SAE paper 950784.

Zhao F-Q; Bai L; Liu Y; Chue T-H; Lai M-C (1997) Transient Flow Characteristics Inside the Catalytic Converter of a Firing Gasoline Engine. SAE paper 971014. 175 – 188.

Fig 1 Schematic of test rig used for flow studies

Fig 2 Schematic of catalyst assembly showing an exploded view of the pulse generator. Flow straighteners are shown in the inlet pipe upstream of the diffuser. At the top of the figure are shown typical cells for a ceramic monolith.

Fig 3 Schematic of flow straightener configurations, (A) dual substrate, (B) triple substrate

Fig 4 Typical inlet velocity profiles. The x and y axes refer to the horizontal and vertical axes through the centre of the inlet tube of diameter 48mm. The x axis coincides with the plate edge when the duct hole is half open.

Fig 5 Non-uniformity index, ψ against Re for (A) 152 mm substrate using 60 degree diffuser, (B) 102 mm substrate using 60 degree diffuser and (C) 152 mm substrate using 180 degree diffuser

Fig 6 Velocity profiles at the rear of the substrate for steady state and pulsating flows, Non dimensional velocity=U_{in}/U_e

Fig. 7 Inlet pulse shapes at 16, 32, 64 and 100 Hz at Re~40000

Fig 8 Exit pulse shapes 20 mm from the wall and on the axis for (A) 16 Hz at Re of 36200, (B) 32 Hz at Re of 43800, (C) 64 Hz at Re of 41100 and (D) 100 Hz at Re of 44700

Fig. 9 Inlet pulse shapes at 32 Hz at Re~20000, 40000, 60000 and 80000

Fig 10 Exit pulse shapes 20 mm from the wall and on the axis at 32 Hz at Re of (A) 18500, (B) 43800, (C) 72000 and (D) 86000

Fig 11 (A) Pressure drop trace and inlet velocity and (B) mean pressure drop as a function of frequency and Re

Fig 12 (A) Inlet pulse shape from ensemble averaged velocity and (B) velocity profiles at the rear of the substrate at 32 Hz

Fig 13 (A) Inlet pulse shape from ensemble averaged velocity and (B) velocity profiles at the rear of the substrate at 100 Hz

Fig 14 Non-uniformity index against non-dimensional parameter, J for (A) 180 degree diffuser and (B) 60 degree diffuser using 152 mm substrate

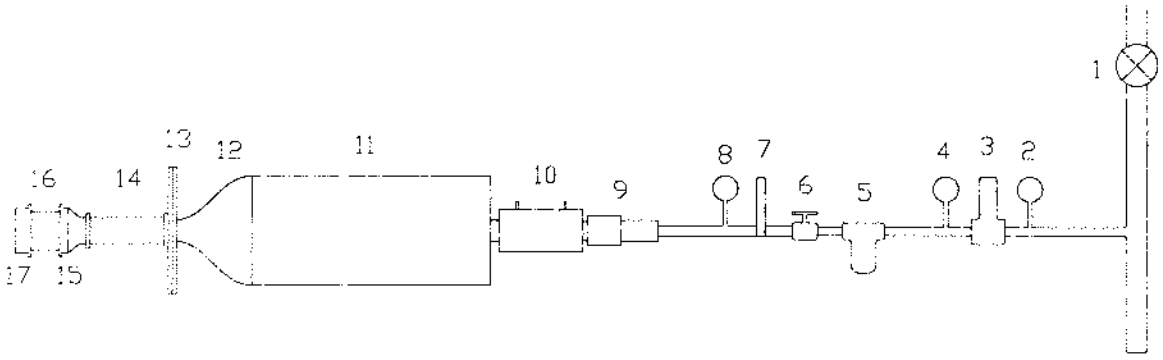
1
2
3
4
5
6
7
8
9
10
11
12
13
14
15
16
17

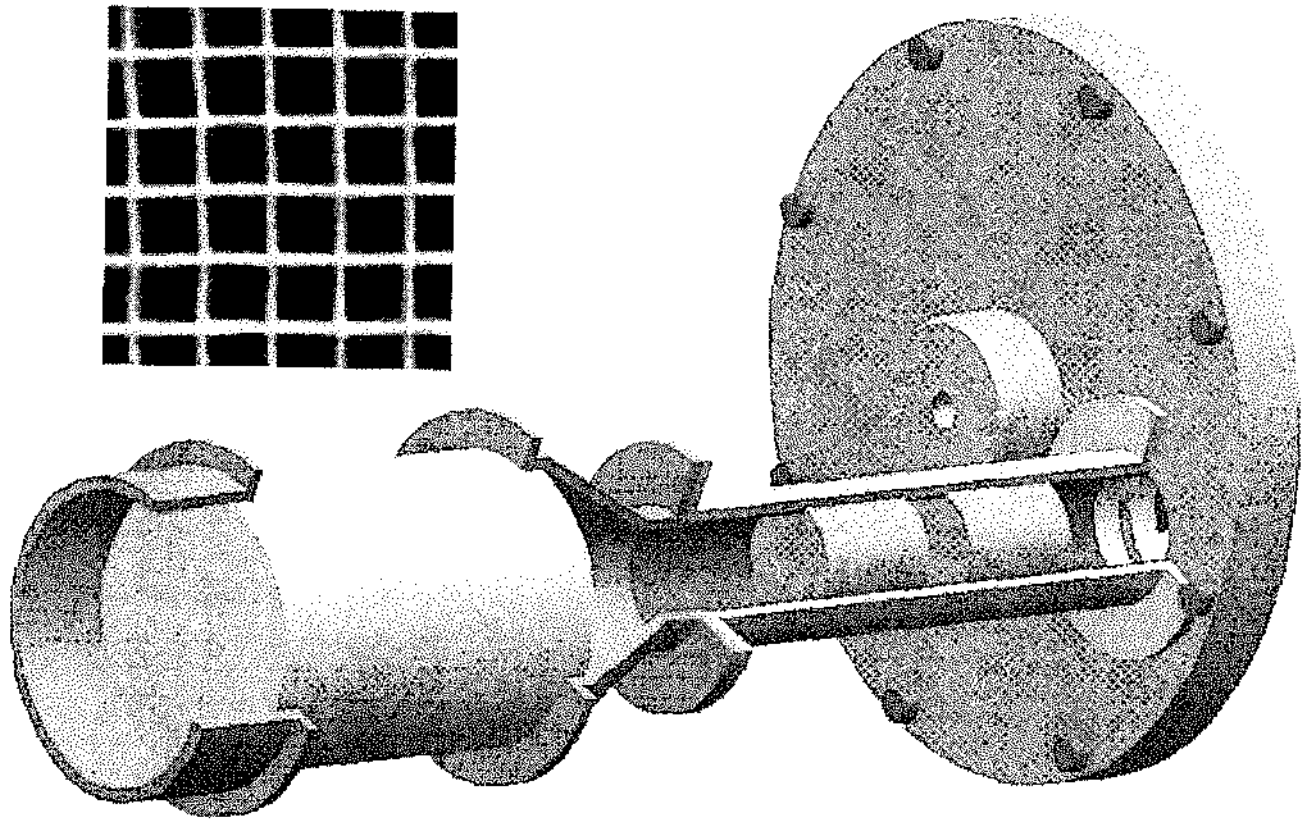

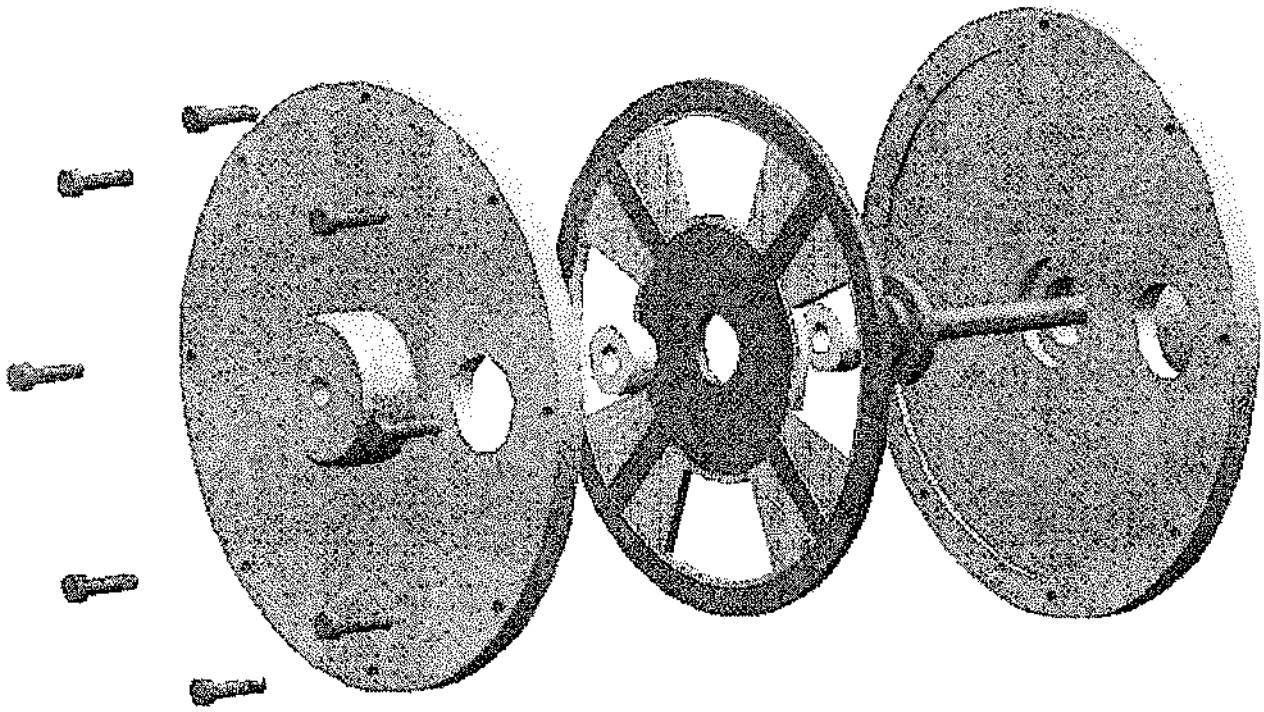

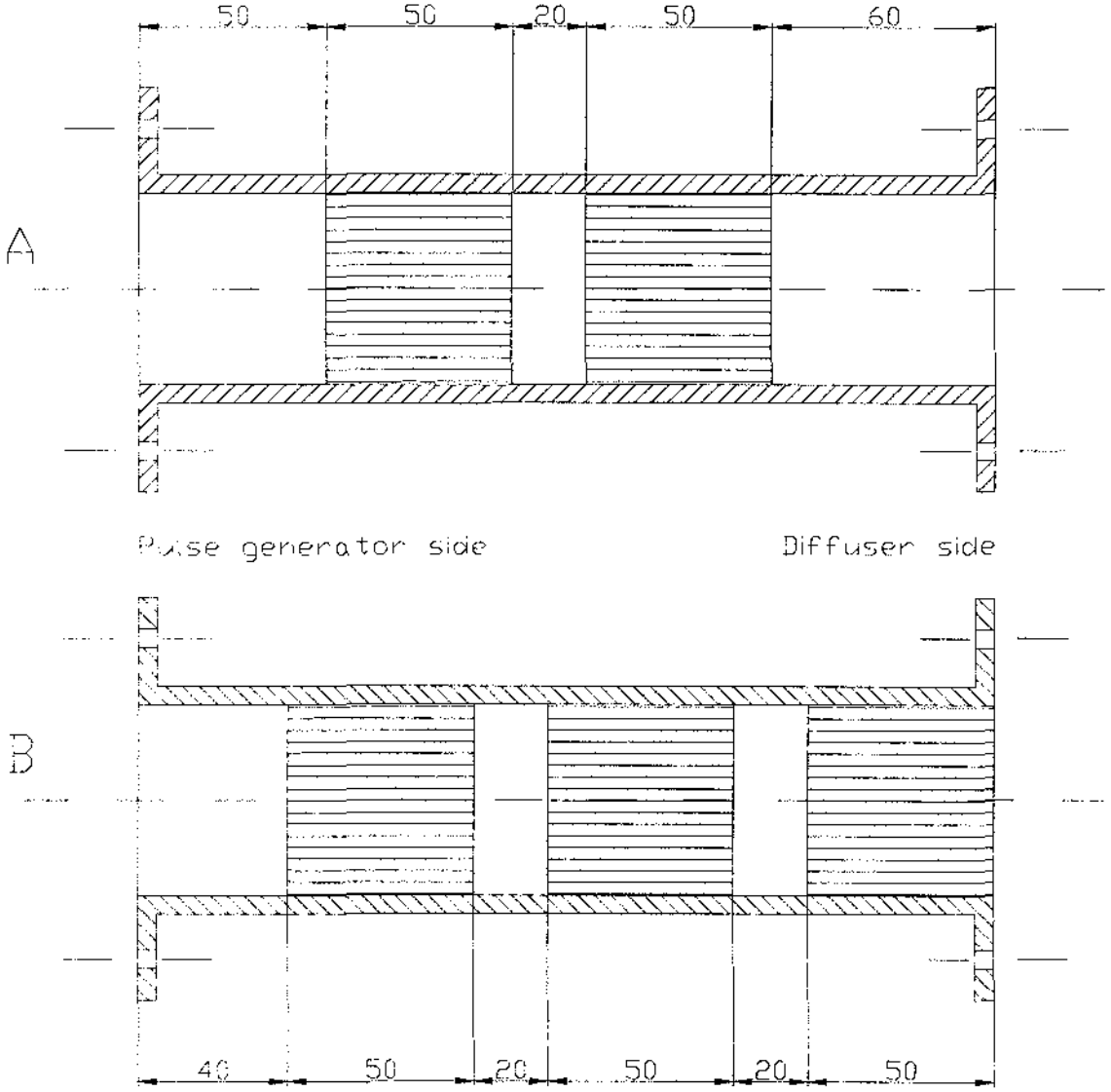
A
50
50
20
50
60
Pulse generator side
Diffuser side
B
40
50
20
50
20
50

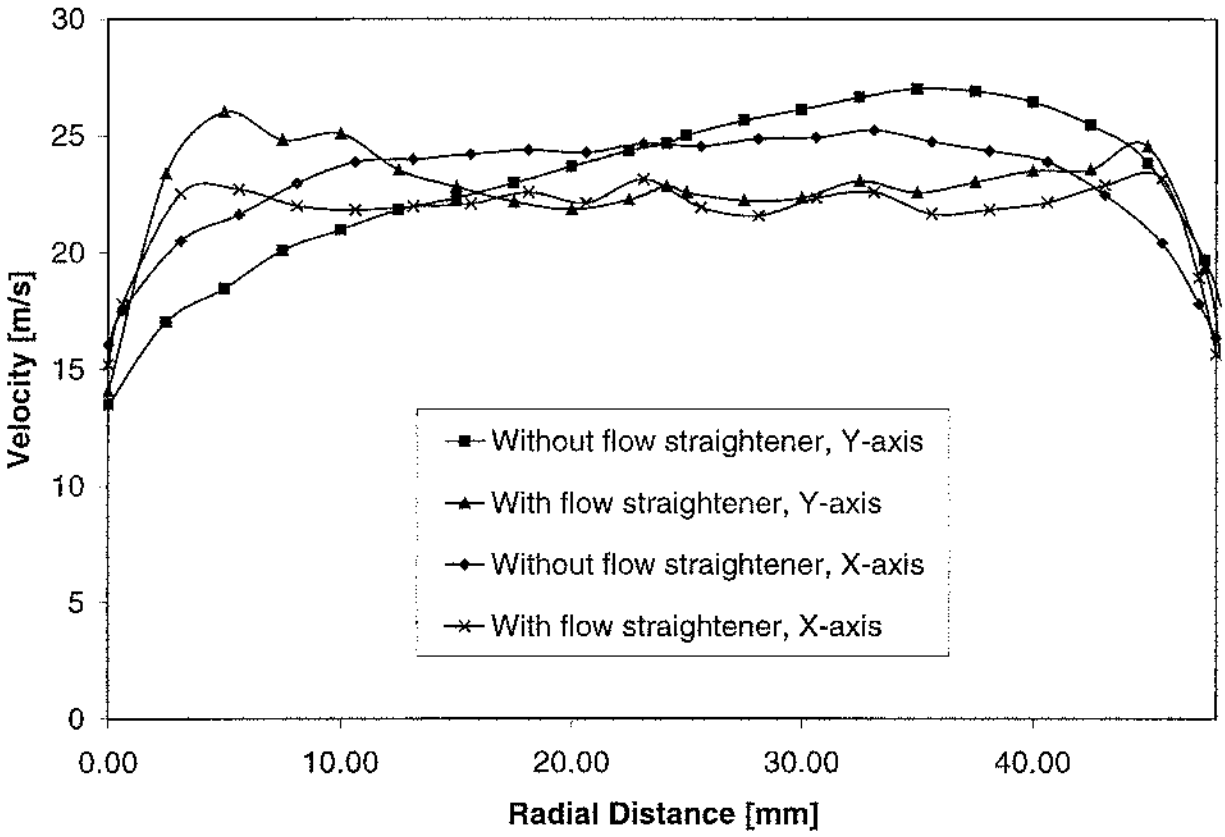
30
25
20
15
10
5
0
Velocity [m/s]
0.00
10.00
20.00
30.00
40.00
Radial Distance [mm]
Without flow straightener, Y-axis
With flow straightener, Y-axis
Without flow straightener, X-axis
With flow straightener, X-axis

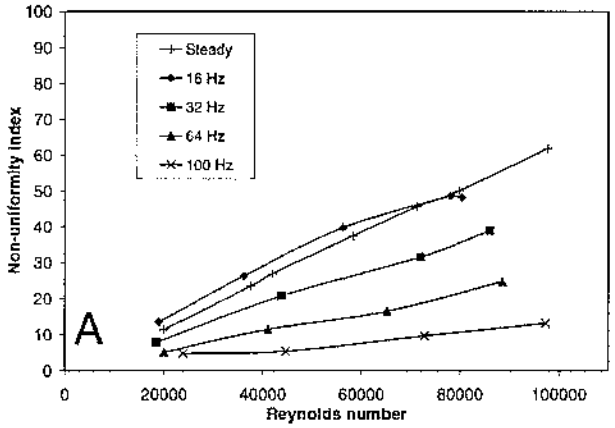
Steady
16 Hz
32 Hz
64 Hz
100 Hz
A
Non-uniformity index
Reynolds number
0
10
20
30
40
50
60
70
80
90
100
0
20000
40000
60000
80000
100000

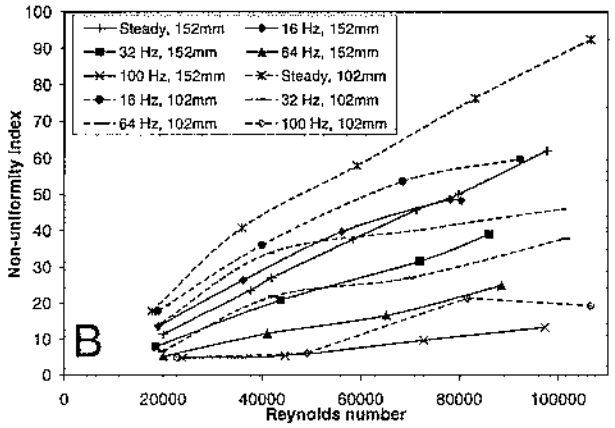
Steady, 152mm
16 Hz, 152mm
32 Hz, 152mm
64 Hz, 152mm
100 Hz, 152mm
Steady, 102mm
16 Hz, 102mm
32 Hz, 102mm
64 Hz, 102mm
100 Hz, 102mm
B
Non-uniformity index
Reynolds number
0
10
20
30
40
50
60
70
80
90
100
0
20000
40000
60000
80000
100000

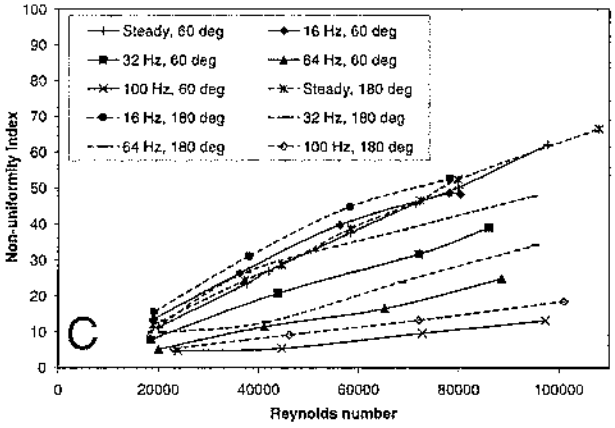
Steady, 60 deg
16 Hz, 60 deg
32 Hz, 60 deg
64 Hz, 60 deg
100 Hz, 60 deg
Steady, 180 deg
16 Hz, 180 deg
32 Hz, 180 deg
64 Hz, 180 deg
100 Hz, 180 deg
C
Non-uniformity index
Reynolds number
0
10
20
30
40
50
60
70
80
90
100
0
20000
40000
60000
80000
100000

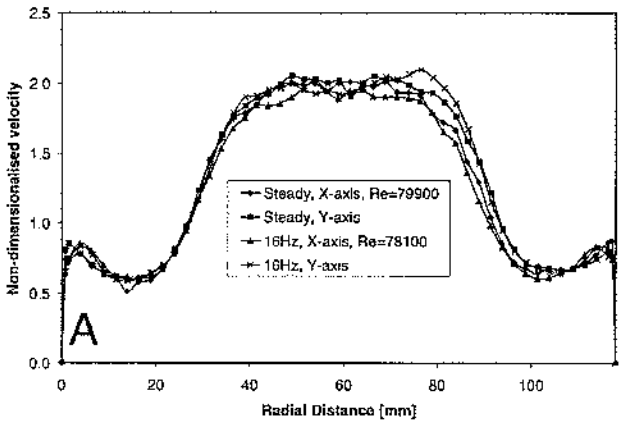
Non-dimensionalised velocity
Radial Distance [mm]
Steady, X-axis, Re=79900
Steady, Y-axis
16Hz, X-axis, Re=78100
16Hz, Y-axis
A

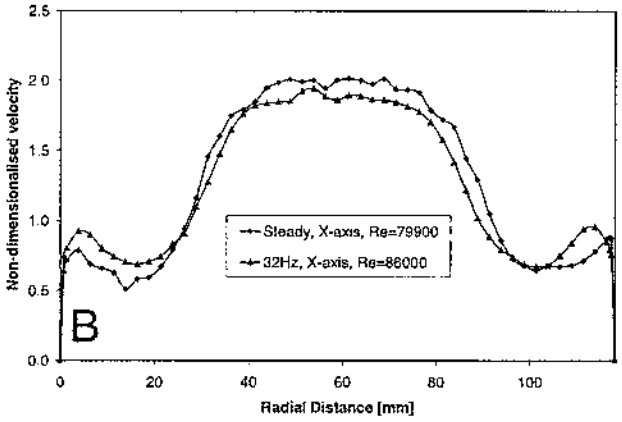
Non-dimensionalised velocity
Radial Distance [mm]
Steady, X-axis, Re=79900
32Hz, X-axis, Re=86000
B

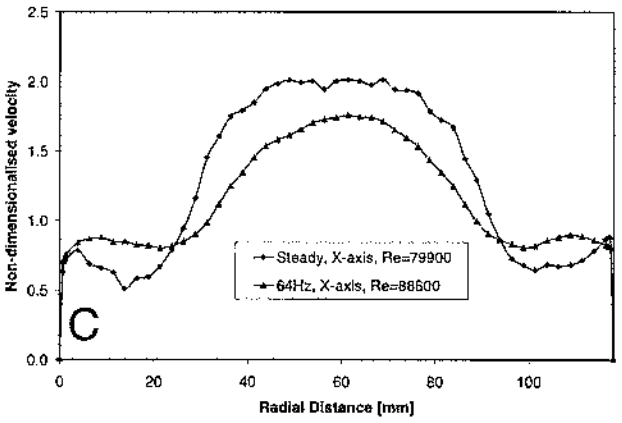
Non-dimensionalised velocity
Radial Distance [mm]
Steady, X-axis, Re=79900
64Hz, X-axis, Re=86600
C

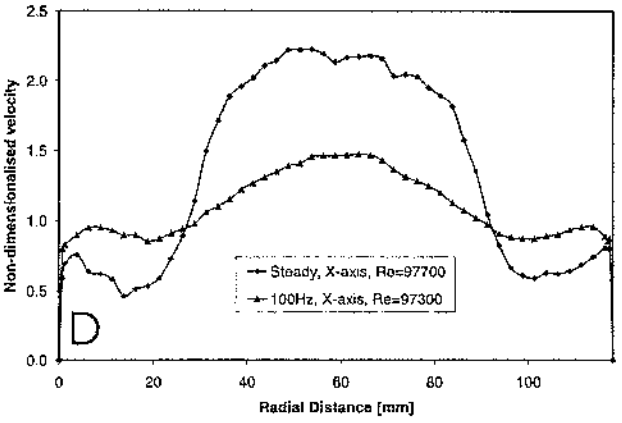
Non-dimensionalised velocity
Radial Distance [mm]
Steady, X-axis, Re=97700
100Hz, X-axis, Re=97300
D

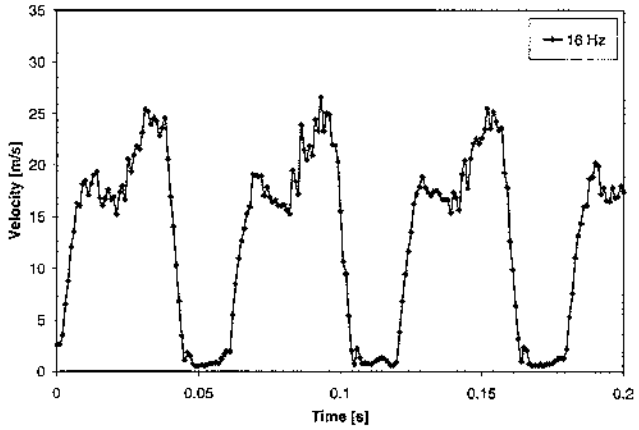
16 Hz
Velocity [m/s]
Time [s]
0
5
10
15
20
25
30
35
0
0.05
0.1
0.15
0.2

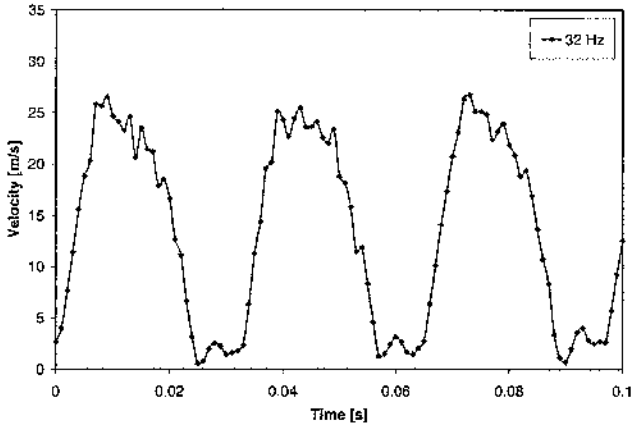
32 Hz
Velocity [m/s]
Time [s]
0
5
10
15
20
25
30
35
0
0.02
0.04
0.06
0.08
0.1

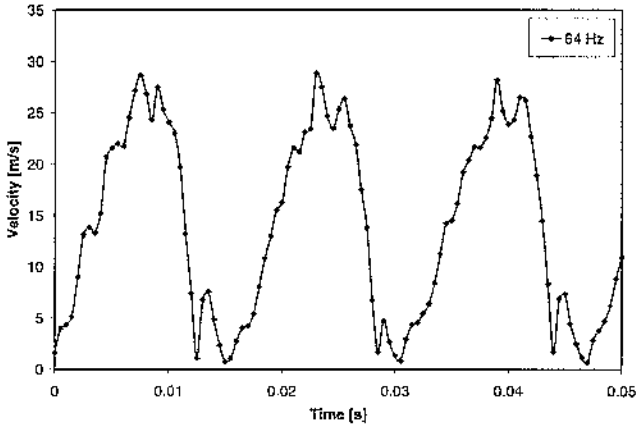
64 Hz
Velocity [m/s]
Time [s]
0
5
10
15
20
25
30
35
0
0.01
0.02
0.03
0.04
0.05

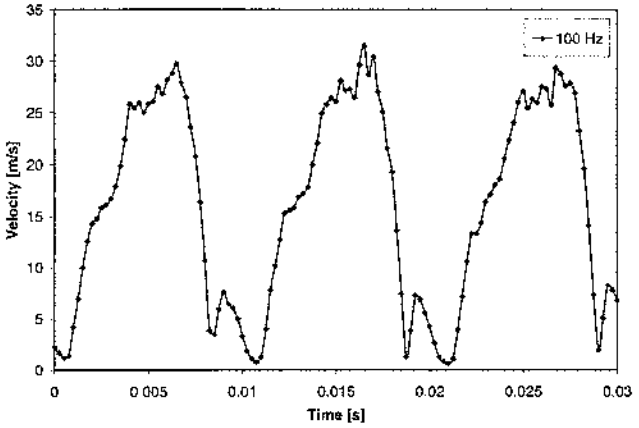
100 Hz
Velocity [m/s]
Time [s]
0
5
10
15
20
25
30
35
0
0.005
0.01
0.015
0.02
0.025
0.03

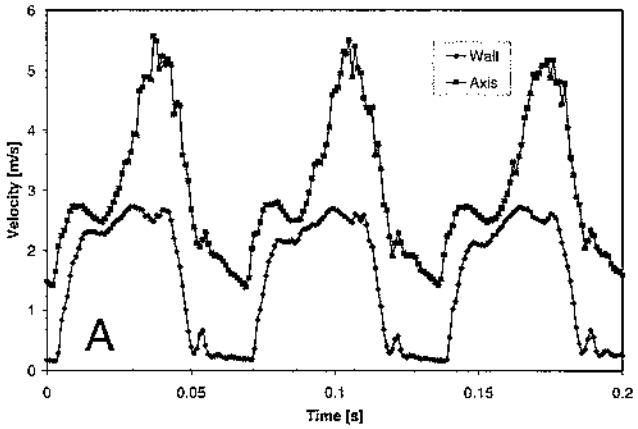
Wall
Axis
Velocity [m/s]
Time [s]
A

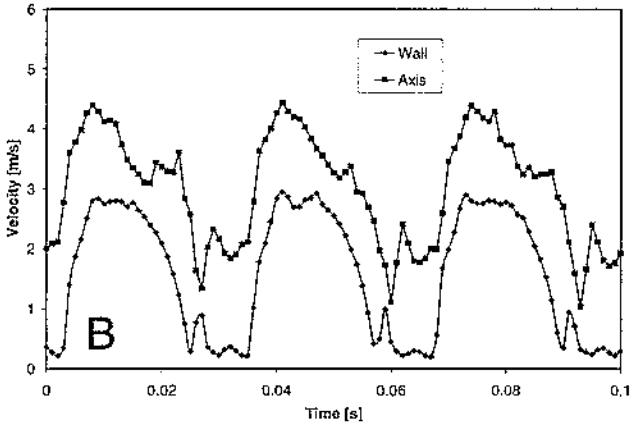
Wall
Axis
Velocity [m/s]
Time [s]
B

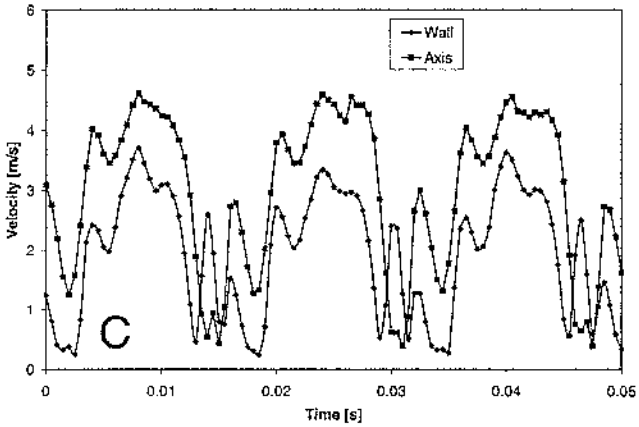
Wall
Axis
Velocity [m/s]
Time [s]
C

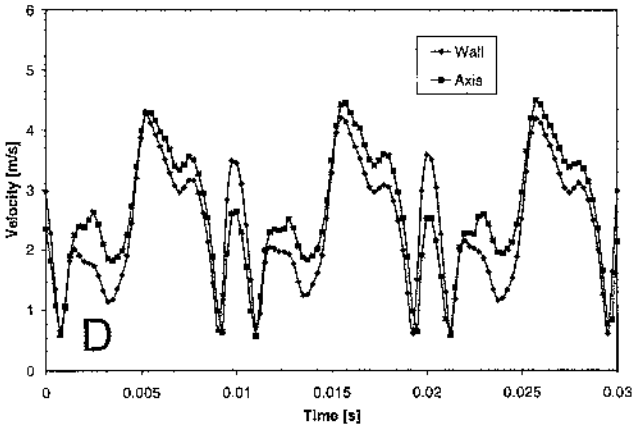
Wall
Axis
Velocity [m/s]
Time [s]
D

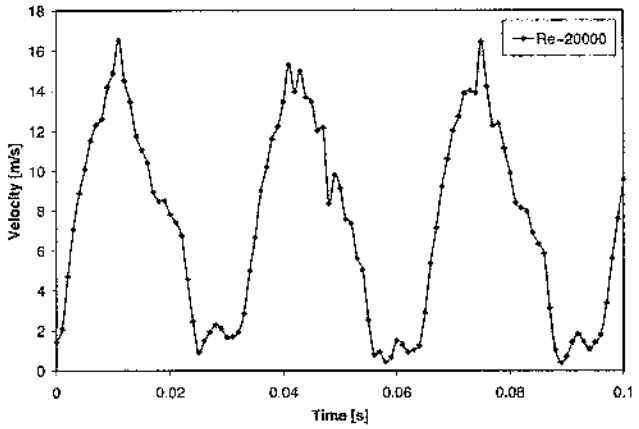
Re~20000
Velocity [m/s]
Time [s]

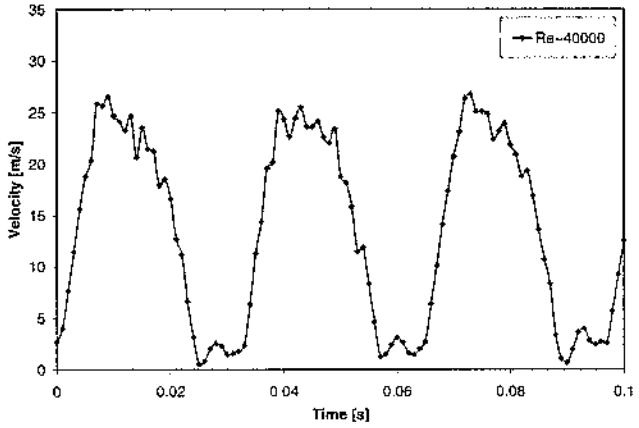
Re~40000
Velocity [m/s]
Time [s]

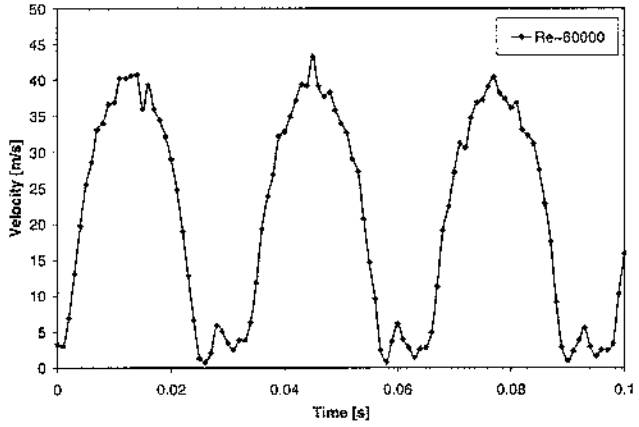
Re~60000
Velocity [m/s]
Time [s]

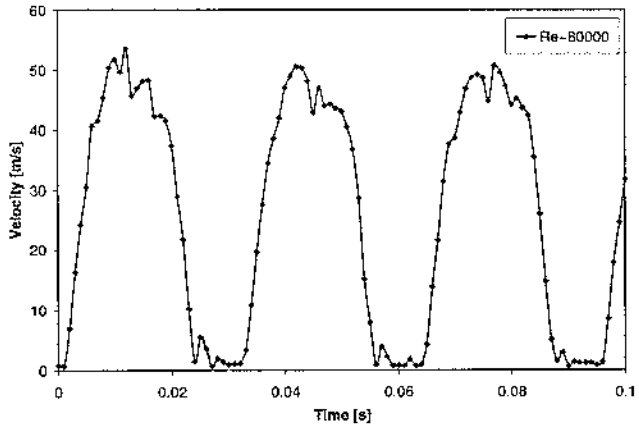
Re~80000
Velocity [m/s]
Time [s]

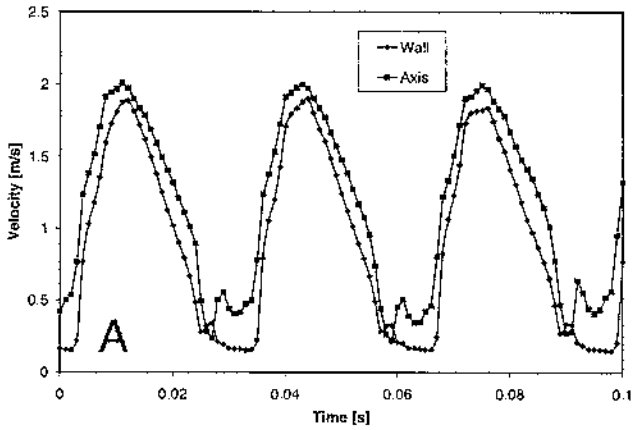
Wall
Axis
Velocity [m/s]
Time [s]
A

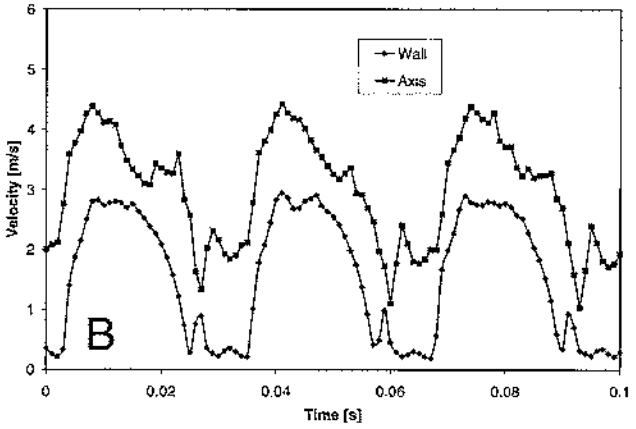
Wall
Axis
Velocity [m/s]
Time [s]
B

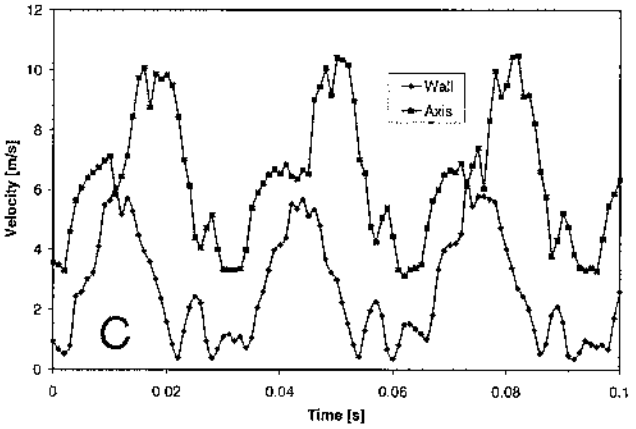
Wall
Axis
Velocity [m/s]
Time [s]
C

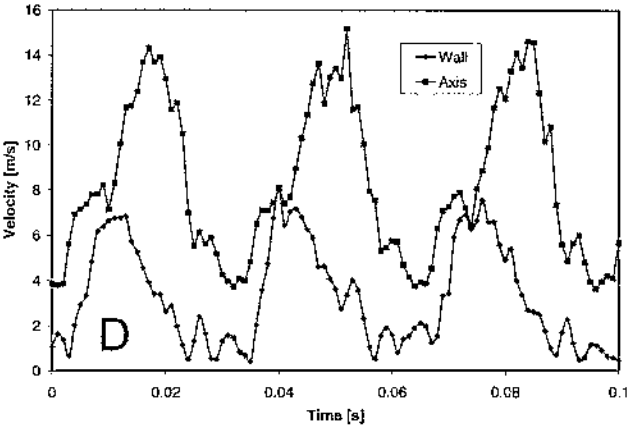
Wall
Axis
Velocity [m/s]
Time [s]
D

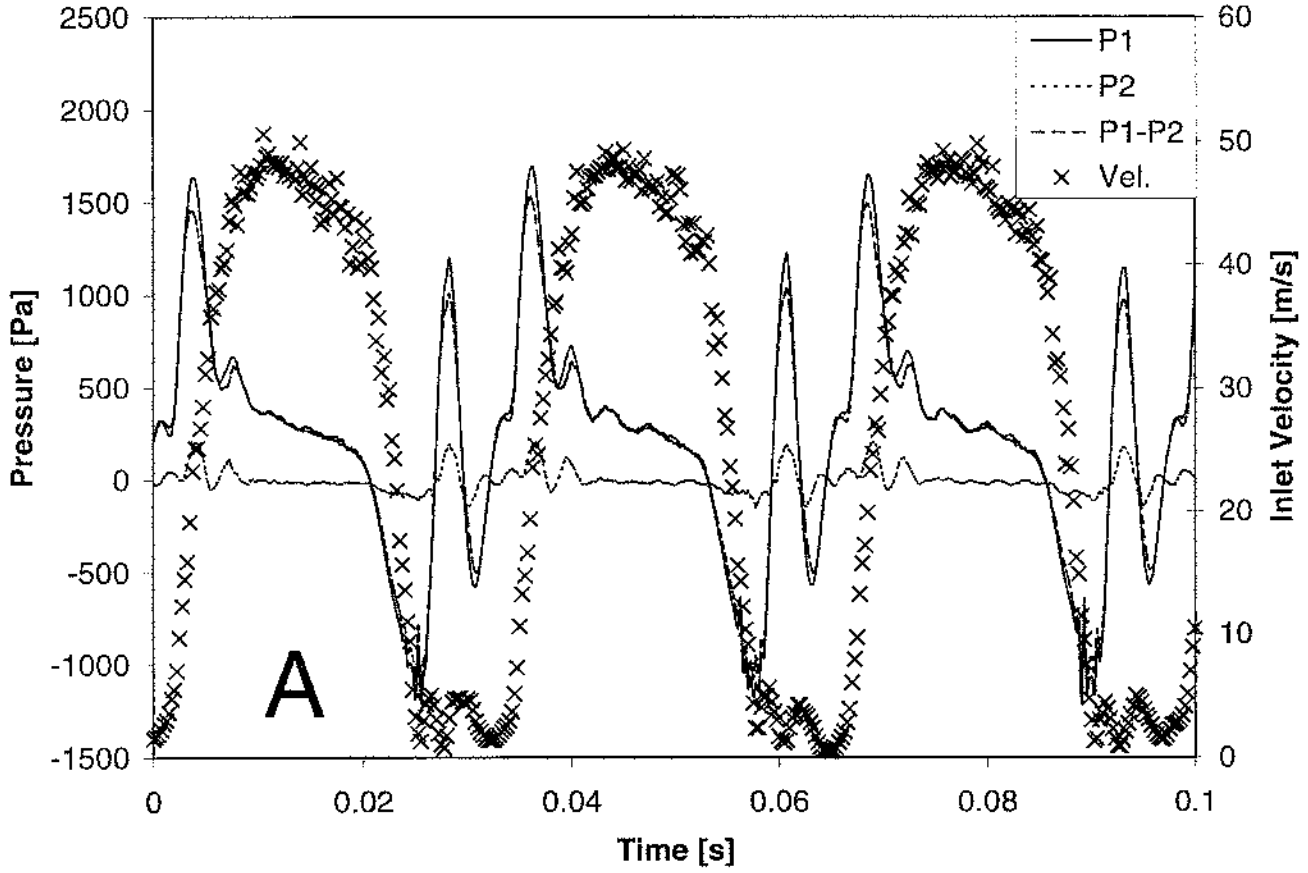
2500
2000
1500
1000
500
0
-500
-1000
-1500
Pressure [Pa]
60
50
40
30
20
10
0
Inlet Velocity [m/s]
P1
P2
P1-P2
Vel.
A
0
0.02
0.04
0.06
0.08
0.1
Time [s]

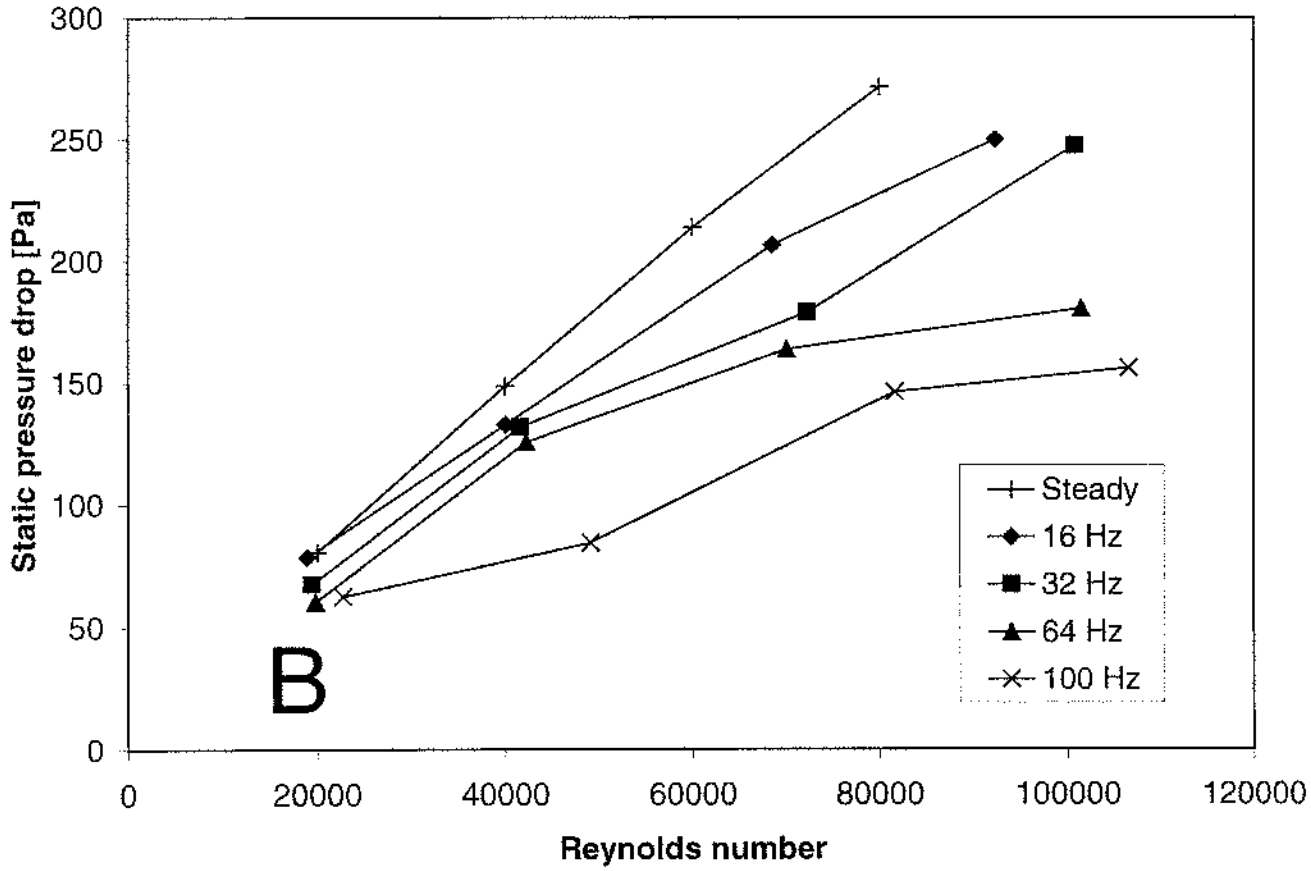
300
250
200
150
100
50
0
Static pressure drop [Pa]
Steady
16 Hz
32 Hz
64 Hz
100 Hz
B
0
20000
40000
60000
80000
100000
120000
Reynolds number

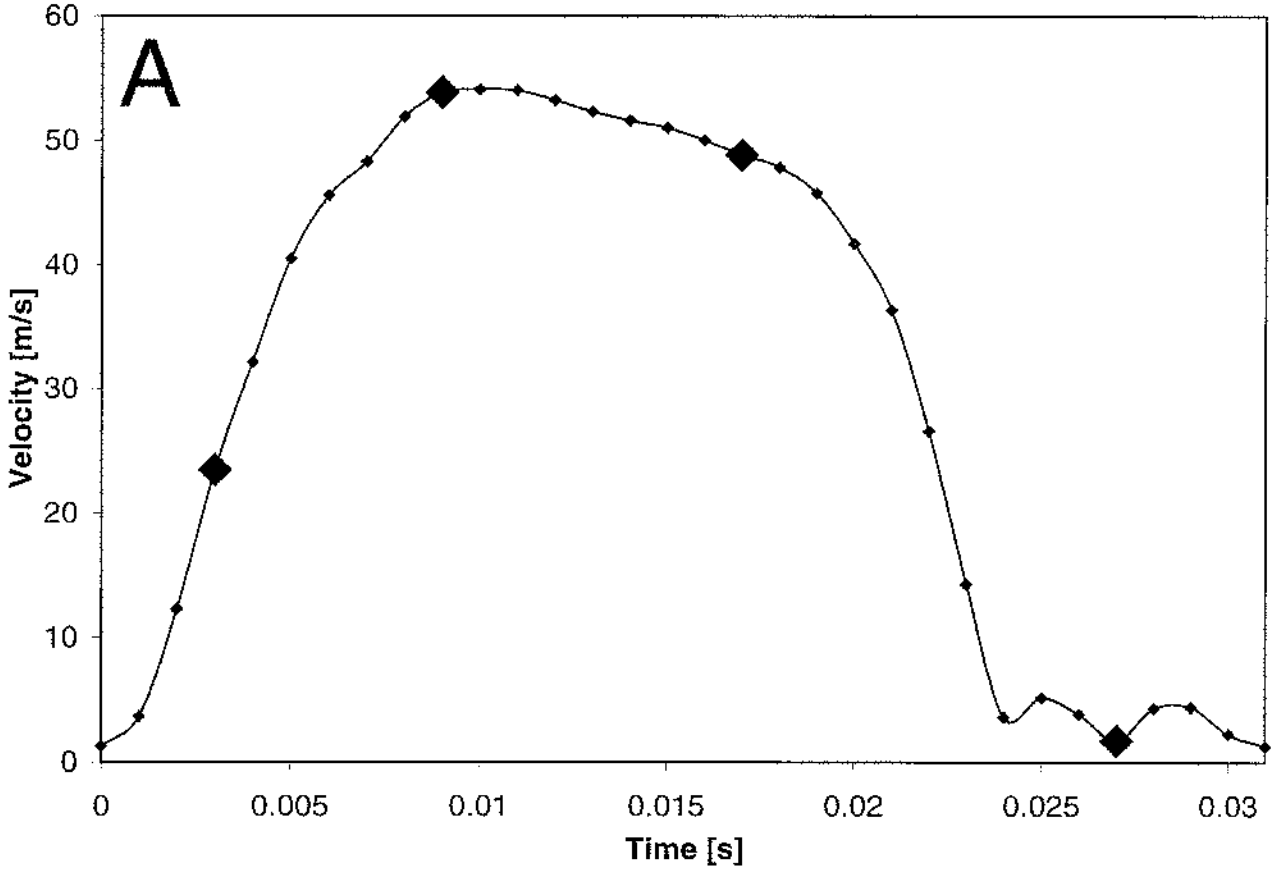
A
Velocity [m/s]
Time [s]
0
10
20
30
40
50
60
0
0.005
0.01
0.015
0.02
0.025
0.03

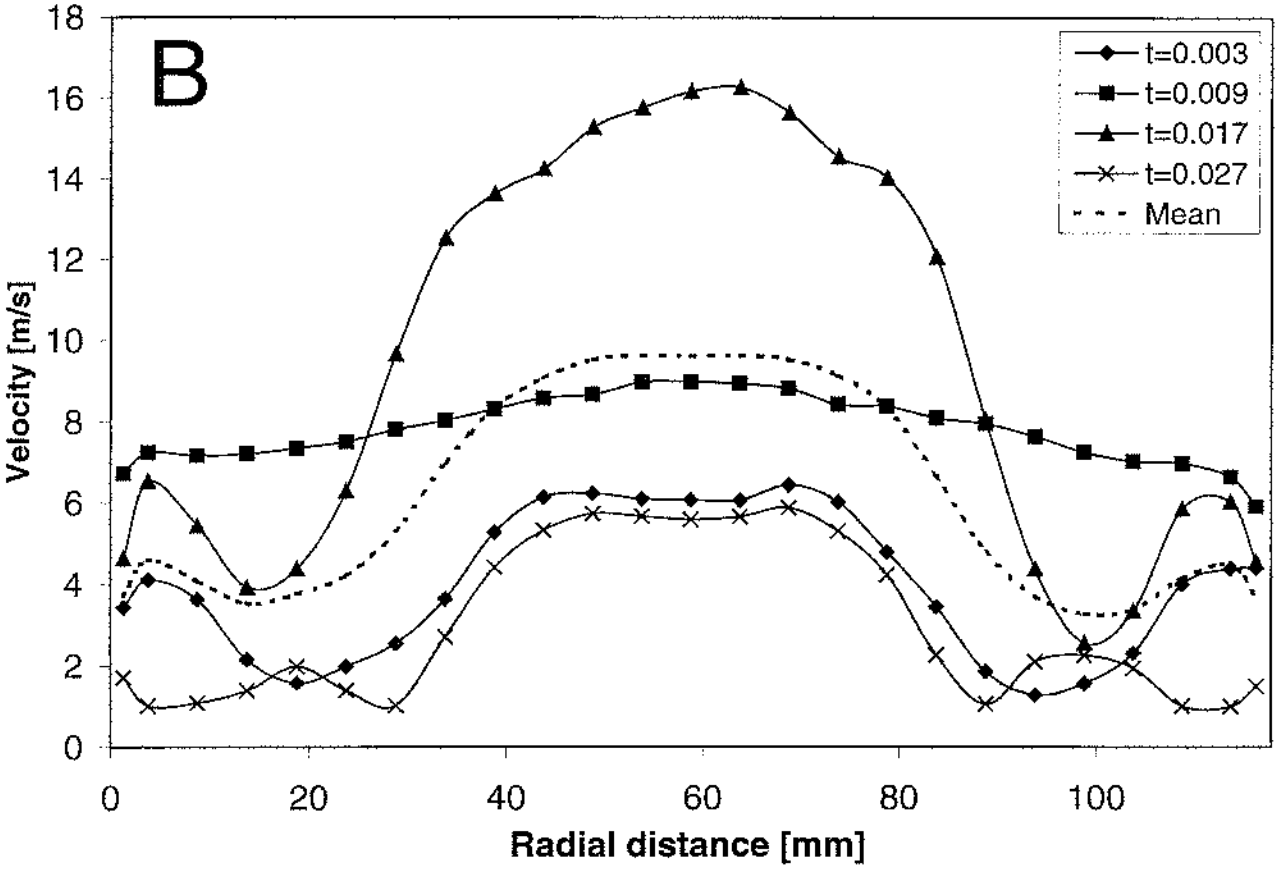
B
t=0.003
t=0.009
t=0.017
t=0.027
Mean
Velocity [m/s]
Radial distance [mm]
0
2
4
6
8
10
12
14
16
18
0
20
40
60
80
100

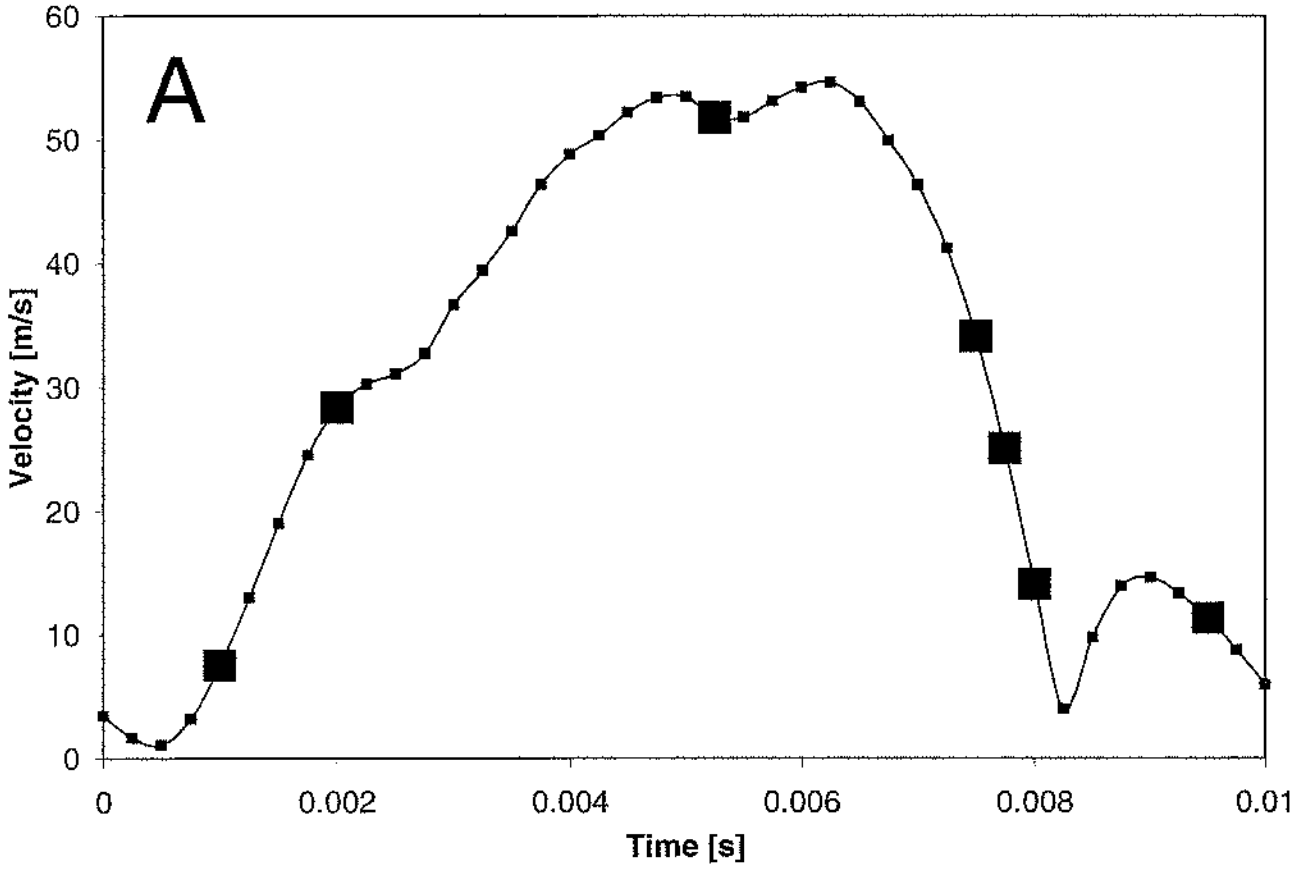
A
Velocity [m/s]
Time [s]
0
10
20
30
40
50
60
0
0.002
0.004
0.006
0.008
0.01

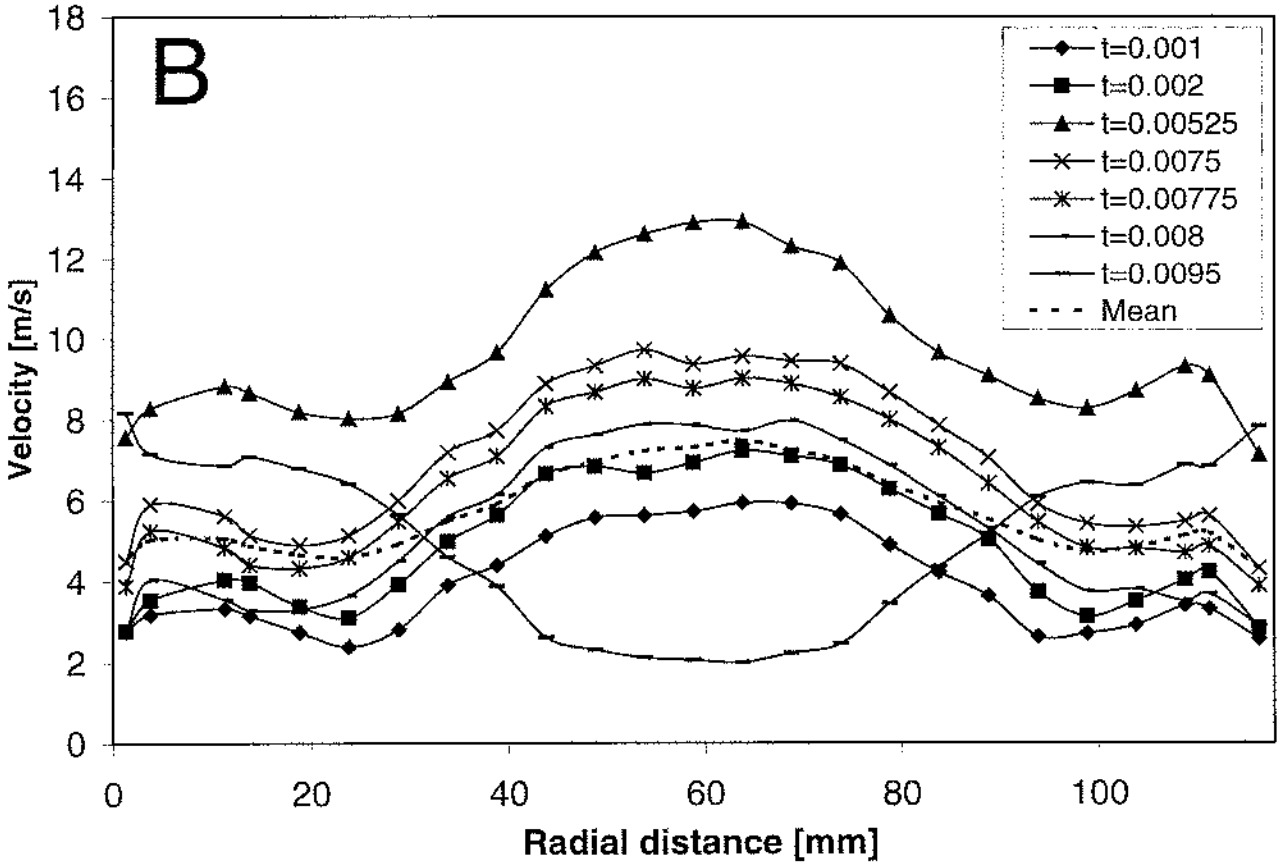
B
Velocity [m/s]
Radial distance [mm]
t=0.001
t=0.002
t=0.00525
t=0.0075
t=0.00775
t=0.008
t=0.0095
Mean
0
2
4
6
8
10
12
14
16
18
0
20
40
60
80
100

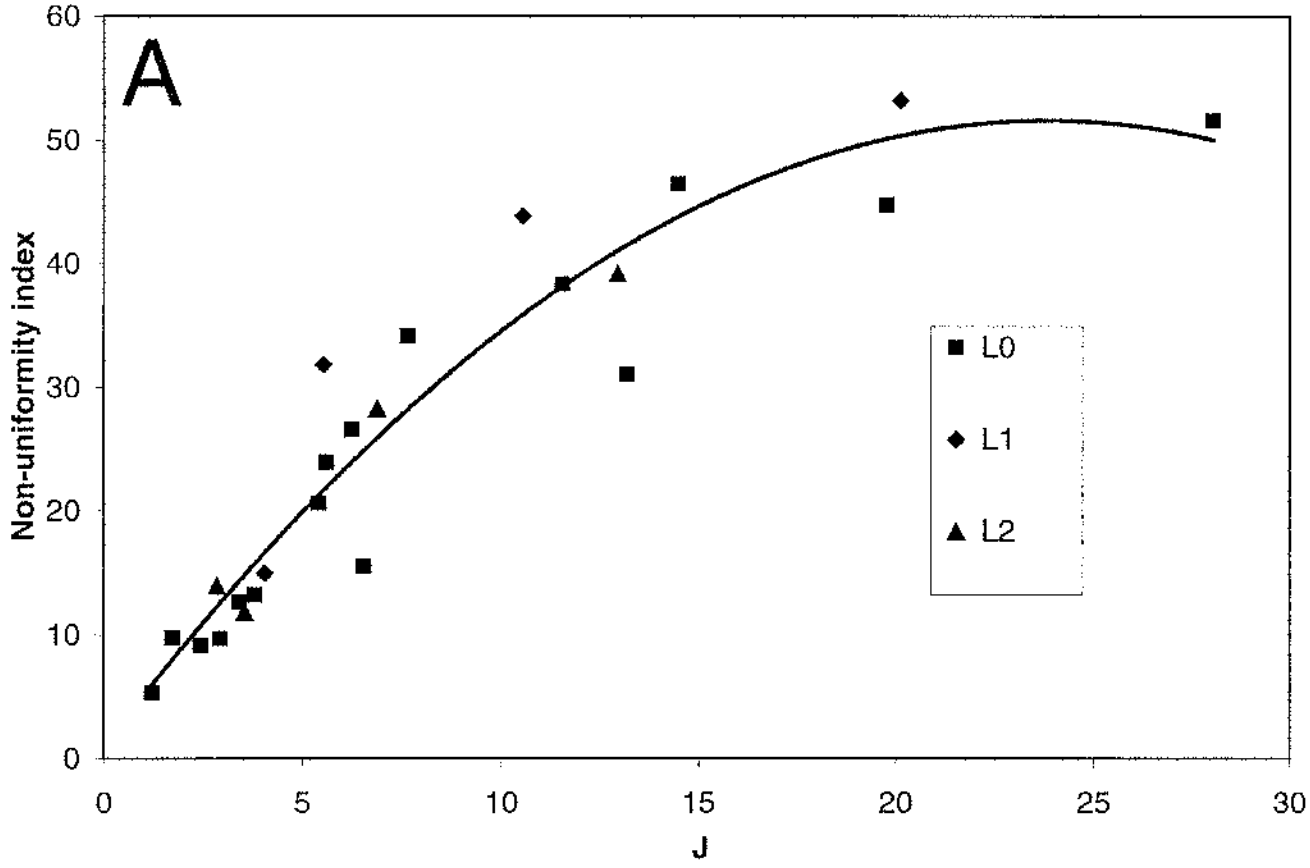
A
Non-uniformity index
J
L0
L1
L2
0
10
20
30
40
50
60
0
5
10
15
20
25
30

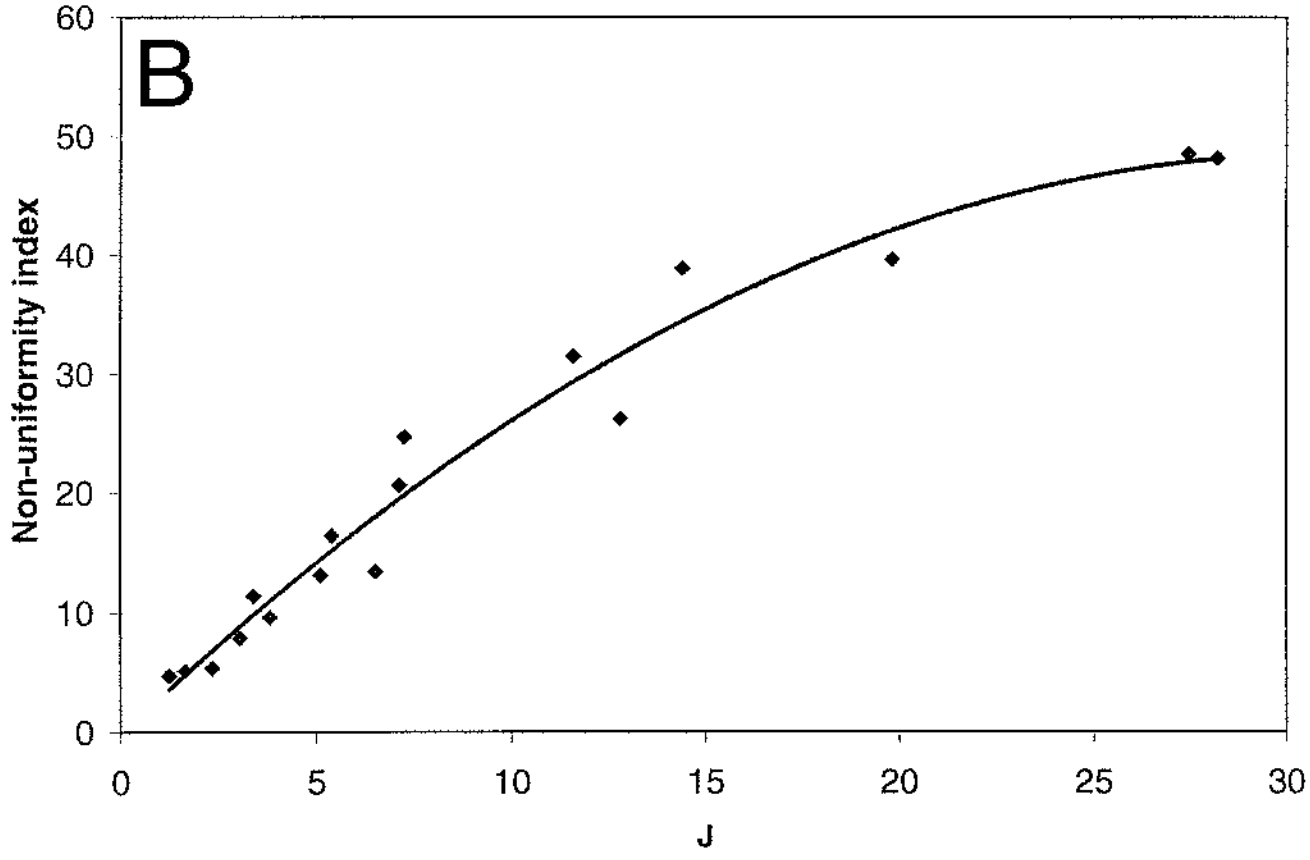
B
Non-uniformity index
J
0
10
20
30
40
50
60
0
5
10
15
20
25
30

Fig 1 Schematic of test rig used for flow studies

Fig 2 Schematic of catalyst assembly showing an exploded view of the pulse generator. Flow straighteners are shown in the inlet pipe upstream of the diffuser. At the top of the figure are shown typical cells for a ceramic monolith.

Fig 3 Schematic of flow straightener configurations, (A) dual substrate, (B) triple substrate

Fig 4 Typical inlet velocity profiles. The x and y axes refer to the horizontal and vertical axes through the centre of the inlet tube of diameter 48mm. The x axis coincides with the plate edge when the duct hole is half open.

Fig 5 Non-uniformity index, ψ against Re for (A) 152 mm substrate using 60 degree diffuser, (B) 102 mm substrate using 60 degree diffuser and (C) 152 mm substrate using 180 degree diffuser

Fig 6 Velocity profiles at the rear of the substrate for steady state and pulsating flows, Non dimensional velocity=U_{in}/U_e

Fig. 7 Inlet pulse shapes at 16, 32, 64 and 100 Hz at Re~40000

Fig 8 Exit pulse shapes 20 mm from the wall and on the axis for (A) 16 Hz at Re of 36200, (B) 32 Hz at Re of 43800, (C) 64 Hz at Re of 41100 and (D) 100 Hz at Re of 44700

Fig. 9 Inlet pulse shapes at 32 Hz at Re~20000, 40000, 60000 and 80000

Fig 10 Exit pulse shapes 20 mm from the wall and on the axis at 32 Hz at Re of (A) 18500, (B) 43800, (C) 72000 and (D) 86000

Fig 11 (A) Pressure drop trace and inlet velocity and (B) mean pressure drop as a function of frequency and Re

Fig 12 (A) Inlet pulse shape from ensemble averaged velocity and (B) velocity profiles at the rear of the substrate at 32 Hz

Fig 13 (A) Inlet pulse shape from ensemble averaged velocity and (B) velocity profiles at the rear of the substrate at 100 Hz

Fig 14 Non-uniformity index against non-dimensional parameter, J for (A) 180 degree diffuser and (B) 60 degree diffuser using 152 mm substrate